

Four-wave mixing in a three-level system interacting with an intense two-frequency pump wave

Motowo Tsukakoshi

RIKEN (Institute of Physical and Chemical Research), Hirosawa, Wako, Saitama 351-01, Japan

(Received 9 August 1988; revised manuscript received 3 April 1989)

A semiclassical treatment of four-wave mixing is presented for the case for which a two-frequency pump wave of arbitrary intensity and a weak probe wave interact with a three-level system. Numerical, as well as analytical, results for the emission spectra are obtained from the steady-state response. At high pump power, the spectra are strongly modified by the ac Stark effect.

I. INTRODUCTION

Four-wave mixing in a nonlinear medium has a wide variety of applications in light-wave generation^{1,2} as well as spectroscopic techniques.³⁻⁶ The investigation of the properties of the generated waves also reveals fundamental physical phenomena due to higher-order nonlinear processes^{7,8} which cannot be clearly observed by saturation techniques. In this paper we discuss four-wave mixing in a three-level system using a semiclassical theory.

Ducloy and Bloch⁹ analyzed four-wave mixing for a two-frequency pump beam and a probe beam by perturbation calculation to third order in the fields. They obtained a Doppler-free doublet structure which was experimentally demonstrated in iodine.¹⁰

A more general discussion on multiresonance four-wave mixing was given in various multilevel systems for weak pump fields,¹¹ where the ac Stark effect and saturation effects are neglected.

An analysis of degenerate four-wave mixing was presented in a two-level system for arbitrarily strong pump fields.¹²⁻¹⁴ A numerical examination of probe-wave amplification was discussed for various relaxation rates of a two-level system.

Saturation behavior in multiresonance four-wave mixing was also analyzed by calculating emission intensity as a function of the probe detuning. A numerical examination of the line profile shows ac Stark splitting and shifts at a higher pump intensity.¹⁵⁻¹⁷ Some of the results are in good agreement with the experimental results.¹⁷

We extend the four-wave-mixing theory to a three-level system when the pump wave has an arbitrary intensity and is composed of two frequencies of arbitrary frequency separation. The population in the levels coupled to the pump wave coherently rings with the frequency separation of the wave. This situation is similar to that of an atom in an intense laser cavity, where an atomic system interacts with a standing-wave radiation field that can be decomposed to two frequencies.^{18,19} Feldman and Feld¹⁹ expanded density-matrix elements into spatial Fourier components with Doppler-shifted frequencies and obtained solutions in terms of continued fractions. The mathematical treatment may be applied to the atomic interaction with a two-frequency pump wave if the density matrix is expanded in a Fourier series in terms of the

pump-frequency difference.

In Sec. II expressions for the nonlinear response are given for a three-level system coupled to a two-frequency pump wave and a weak probe wave. In Sec. III we present results of the numerical evaluation for special cases of interest, and display the response graphically, and then interpret the results that come from different physical processes. It is found that resonances occur at the center of the probe detuning and a Rabi frequency when the pump intensity is considerably high and the frequency separation is small compared with the relaxation rates of the transition levels.

II. RESPONSE OF A THREE-LEVEL SYSTEM DRIVEN BY A TWO-FREQUENCY PUMP FIELD

We consider a three-level system coupled to an intense pump and a weak probe wave. Figure 1 illustrates four-wave-mixing processes in a three-level-system of an inverted V type. The pump waves $E_1(\omega_1 + \omega)$ and $E'_1(\omega_1 - \omega)$ interact with the 0-1 transition, and the probe frequency ω_2 is tuned near the center frequency of the 1-2 transition. In the process, amplification of the probe wave and emission of a wave with ω_3 occur at the 1-2 transition.

At the end of the process, the atom is transferred to level 2, different from the initial state, level 0.²⁰ In Figs. 1(a) and 1(b), the probe wave is amplified, while a wave at ω_3 , different from ω_2 by 2ω , is generated in the processes shown in Figs. 1(c) and 1(d).

If the pump waves are assumed to have the same amplitude for the simplicity of the calculation, the field is described as

$$E = E_1 \sin(\omega t + \psi) \cos(\omega_1 t + \psi_1) + E_2 \cos(\omega_2 t + \psi_2), \quad (1)$$

where ψ , ψ_1 , and ψ_2 are the initial phases of the waves which will be set to zero in the calculation.

The three-level system is influenced by pumping and decay processes as well as the interaction with the fields. The time evolution of the system is described by a density matrix ρ which is subject to the Schrödinger equation

$$\frac{\partial \rho}{\partial t} = [H, \rho] / i\hbar. \quad (2)$$

The total Hamiltonian for the system is

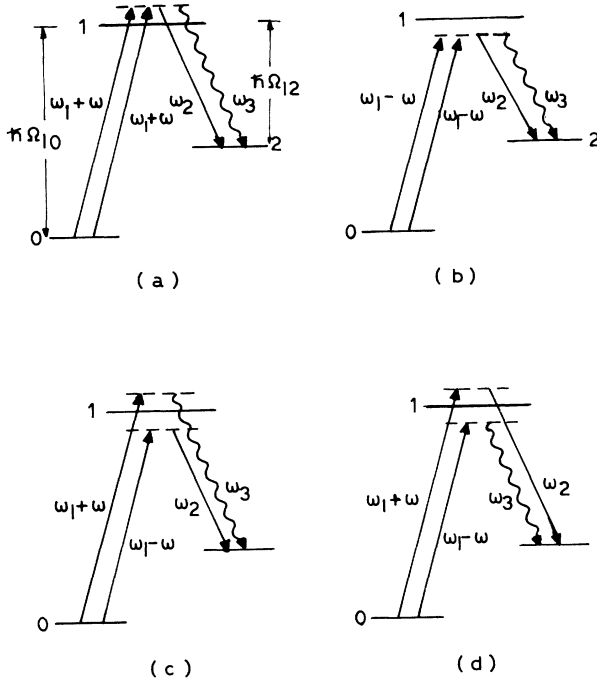


FIG. 1. Schematic representation of various four-wave mixing processes in which a three-level system interacts with a two-frequency pump wave at $\omega_1 \pm \omega$, and a probe wave at ω_2 .

$$H = H_0 - p \cdot E, \quad (3)$$

where H_0 is the unperturbed Hamiltonian and p is the transition dipole moment.

In the electric dipole approximation, the density-matrix elements follow the equation of motion,

$$\dot{\rho}_{00} = -\gamma_0(\rho_{00} - N_0) + iV_1(\rho_{10} - \rho_{10}^*), \quad (4a)$$

$$\dot{\rho}_{11} = -\gamma_1\rho_{11} - iV_1(\rho_{10} - \rho_{10}^*) + iV_2(\rho_{21} - \rho_{21}^*), \quad (4b)$$

$$\dot{\rho}_{22} = -\gamma_2\rho_{22} - iV_2(\rho_{21} - \rho_{21}^*), \quad (4c)$$

$$\dot{\rho}_{10} = -(\gamma_{10} + i\Omega_{10})\rho_{10} - iV_1(\rho_{11} - \rho_{00}) + iV_2\rho_{20}, \quad (4d)$$

$$\dot{\rho}_{21} = -(\gamma_{21} + i\Omega_{21})\rho_{21} - iV_2(\rho_{22} - \rho_{11}) - iV_1\rho_{20}, \quad (4e)$$

$$\dot{\rho}_{20} = -(\gamma_{20} + i\Omega_{20})\rho_{20} - iV_1\rho_{21} - iV_2\rho_{10}, \quad (4f)$$

$$\rho_{ij} = \rho_{ji}^* \quad (i, j = 0, 1, 2), \quad (4g)$$

$$V_1 = (\mu_{10}E_1/\hbar)\sin(\omega t + \psi)\cos(\omega_1 t + \psi_1), \quad (4h)$$

$$V_2 = (\mu_{21}E_2/\hbar)\cos(\omega_2 t + \psi_2), \quad (4i)$$

where Ω_{ij} is the atomic resonance frequency for the i - j transition, γ_i is the decay rate of level i , γ_{ij} is the dephasing rate of the polarization for the levels i and j , and nonzero transition dipole moments are μ_{10} and μ_{21} .

We have an interest in the optical wave generation by four-wave mixing near frequency ω_2 . The field strength of the wave E_i ($i=2,3$), in the slowly varying envelope approximation, is given by

$$\frac{dE_i}{dz} = -\frac{1}{2} \frac{\omega_i \mu_{21}}{c \epsilon_0} \text{Im} \rho_{21} \quad (i=2 \text{ or } 3) \quad (5)$$

when the wave propagated along the z axis. To investigate the features of the generated waves we should calculate the imaginary part of the density-matrix element ρ_{21} .

We first solve ρ_{00} , ρ_{10} , and ρ_{11} to all orders of E_1 . Then the solutions can be obtained by iteration between the diagonal and off-diagonal elements. When the atoms have initially diagonal elements, the off-diagonal elements have Fourier components at ω through V_1 . Then, the diagonal elements oscillate at 2ω through the interaction V_1 , and so forth. In this way, the off-diagonal elements oscillate at $(2n+1)\omega$, where n is an integer.

Thus the matrix elements can be expanded as

$$\rho_{00} = \sum_n (p_n e^{2in\omega t} + p_n^* e^{-2in\omega t}), \quad (6a)$$

$$\rho_{11} = \sum_n (P_n e^{2in\omega t} + P_n^* e^{-2in\omega t}), \quad (6b)$$

$$\rho_{10} = \exp(-i\omega_1 t) \sum_n (q_{2n+1} e^{i(2n+1)\omega t} + q_{-(2n+1)} e^{-i(2n+1)\omega t}). \quad (6c)$$

Combining Eqs. (4) and (6), we have the expressions

$$\rho_{21} = \exp(-i\omega_2 t) \sum_n (r_{2n} e^{2in\omega t} + r_{-2n} e^{-2in\omega t}), \quad (7a)$$

$$\rho_{20} = \exp[-i(\omega_1 + \omega_2)t] \sum_n (s_{2n+1} e^{i(2n+1)\omega t} + s_{-(2n+1)} e^{-i(2n+1)\omega t}). \quad (7b)$$

Inserting Eqs. (6) and (7) into Eqs. (4a)–(4b), we have coupled equations for the Fourier amplitudes. These coupled equations may be rearranged by using the following notation:

$$\alpha_n = p_n - P_n, \quad n \text{ even} \quad (8)$$

$$\alpha_n = q_n - q_{-n}, \quad n \text{ odd}$$

$$\beta_n = r_n, \quad n \text{ even} \quad (9)$$

$$\beta_n = s_n, \quad n \text{ odd}.$$

Thus we obtain a set of coupled linear equations

$$\alpha_{n+1} + a_n \alpha_n - \alpha_{n-1} = a_n \delta_{n0}, \quad (10a)$$

$$\beta_{n+1} + b_n \beta_n - \beta_{n-1} = \phi_n, \quad (10b)$$

where

$$a_n = [1/(\gamma_0 + in\omega) + 1/(\gamma_1 + in\omega)]^{-1} V_{10}, \quad n \text{ even} \quad (11)$$

$$a_n = \{1/[\gamma_{10} + i(\Delta_1 + n\omega)]$$

$$+ 1/[\gamma_{10} + i(\Delta_1 - n\omega)]\}^{-1} V_{10}, \quad n \text{ odd}$$

$$b_n = -[\gamma_{21} + i(\Delta_2 + n\omega)]/V_{10}, \quad n \text{ even} \quad (12)$$

$$b_n = -[\gamma_{20} + i(\Delta_3 + n\omega)]/V_{10}, \quad n \text{ odd}$$

$$\phi_n = -i(V_{20}/V_{10})P_n, \quad n \text{ even} \quad (13)$$

$$\phi_n = -i(V_{20}/V_{10})q_n, \quad n \text{ odd}$$

where

$$\Delta_1 = \Omega_{10} - \omega_1, \quad \Delta_2 = \Omega_{21} - \omega_2, \quad \Delta_3 = \Delta_1 - \Delta_2, \\ V_{10} = \mu_{10} E_1 / \hbar, \quad V_{20} = \mu_{21} E_2 / \hbar.$$

Equation (10a) may be rewritten in the form

$$u_n = \frac{1}{a_n + u_{n+1}}, \tag{14}$$

where $u_n = \alpha_{n+1} / \alpha_n$.

Using successively the same relation as Eq. (14) for $n+1, n+2, \dots$, we have a continued fraction

$$u_n = \frac{1}{a_n + \frac{1}{a_{n+1} + \frac{1}{a_{n+2} + \dots}}}. \tag{15}$$

From Eq. (10) for $n=0$ and Eq. (15), we have

$$\alpha_0 = \frac{a_0}{a_0 + 2 \operatorname{Im} u_1}. \tag{16}$$

Other α_n may be obtained combining Eqs. (15) and (16).

Next, we solve Eqs. (10b) using α_n obtained above. Because the solution with physical meaning converges as $n \rightarrow \infty$, we will have for large N

$$v_n = \frac{1}{b_n + \frac{1}{b_{n+1} + \frac{1}{b_{n+2} + \dots}}}. \tag{21}$$

Inserting Eqs. (18) and (20) into Eq. (10b), we have successive Fourier amplitudes at higher frequencies.

To obtain the emission intensity, we need to calculate the imaginary part of ρ_{21} which is written from Eqs. (7a) and (9) as

$$\operatorname{Im} \rho_{21} = \operatorname{Im} \beta_0 + \operatorname{Im} [(\beta_2 - \beta_{-2}^*) e^{2i\omega t}] \\ + \operatorname{Im} [(\beta_4 - \beta_{-4}^*) e^{4i\omega t}] + \dots \tag{22}$$

Inserting Eqs. (18) and (20) into Eq. (22) we have the line shape for the generated wave as a function of the probe frequency.

The continued fractions, Eqs. (15) and (21), have simple forms for small $\omega (\ll \gamma_0, \gamma_1, \gamma_2)$. In this case, the coefficients in Eq. (11) will be independent of n as

$$a_n = \frac{\gamma_0 \gamma_1}{2 \gamma_{10} V_{10}} \equiv a_0, \quad n \text{ even} \\ a_n = \frac{\gamma_{10}^2}{2 \gamma_{10} V_{10}} \equiv a_1, \quad n \text{ odd}. \tag{23}$$

Thus we have recurring continued fractions for u_n . The coupled equations (10) are solved by setting

$$\beta_N = 0. \tag{17}$$

Inserting Eq. (17) into Eq. (10b) and taking the iteration procedure, we obtain the Fourier amplitudes of ρ_{21} as

$$\beta_0 = \frac{1}{b_0 + v_1 + v_{-1}} \left[\phi_0 + \sum_{i=1}^N (-1)^i (\phi_i v_i - \phi_{-i} v_{-i}) \right], \tag{18}$$

where

$$\beta_1 = \beta_0 v_1 - \sum_{j=1}^N (-1)^j \phi_j v_j \tag{19}$$

and

$$\beta_2 = (\beta_0 + \phi_1) v_2 + a_1 \sum_{j=2}^N (-1)^j \phi_j v_j, \tag{20a}$$

and

$$\beta_{-2} = (\beta_0 + \phi_{-1}) v_{-2} + a_{-1} \sum_{j=2}^N (-1)^j \phi_{-j} v_{-j}, \tag{20b}$$

where

$$\alpha_n = R^n \alpha_0, \quad n \text{ even} \\ \alpha_n = R^{n-1} \alpha_1, \quad n \text{ odd}. \tag{24}$$

Inserting Eqs. (23) into Eqs. (10), we obtain

$$R = \{2 + [a_0 a_1 (a_0 a_1 + 4)]^{1/2}\} / 2, \tag{25}$$

$$a_0 a_1 = \frac{\gamma_0 \gamma_1}{4 \gamma_{10}^2 V_{10}^2} (\gamma_{10}^2 + \Delta_1^2), \tag{26}$$

$$\alpha_0 = 1 / (1 + 4 V_{10}^2 / \gamma_0 \gamma_1)^{1/2}, \tag{27}$$

and

$$\alpha_1 = (\gamma_0 \gamma_1 / 2 \gamma_{10} V_{10}) [1 - 1 / (1 + 4 V_{10}^2 / \gamma_0 \gamma_1)^{1/2}]. \tag{28}$$

In a similar way, the continued fraction in Eq. (21) is solved at $\Delta_1 = \Delta_2 = 0$ as

$$v_n = r^n v_0, \quad n \text{ even} \tag{29a}$$

$$v_n = r^{n-1} v_1, \quad n \text{ odd} \tag{29b}$$

and

$$r = \{2 + b_0 b_1 \pm [b_0 b_1 (b_0 b_1 + 4)]^{1/2}\} / 2, \tag{30}$$

where $b_0 = \gamma_{21} / V_{10}$ and $b_1 = \gamma_{20} / V_{10}$. Combining Eqs.

(18), (20), (24), and (29), we obtain

$$\beta_0 = i(\Gamma V_{20}/4V_{10}^2)(1/A - 1/B)^{-1} \times [(1+2/A)^{-1/2}(1+2/B)^{-1/2}] \quad (31)$$

and

$$\beta_2 - \beta_{-2}^* = i(\gamma_0 \Gamma V_{20}/2\gamma_{10} V_{10}^2) \times \{1 - (A-B)^{-1}[(1+A)(1+2/A)^{-1/2} - (1+B)(1+2/B)^{-1/2}]\}, \quad (32)$$

where

$$A = 2\gamma_{20}\gamma_{21}/V_{10}^2 \quad (33a)$$

and

$$B = \gamma_0\gamma_1/2V_{10}^2, \quad (33b)$$

with $\Gamma = (\gamma_0 + \gamma_1 + \gamma_2)/2$. β_0 corresponds to the emission intensity at the probe frequency, while $\beta_2 - \beta_{-2}^*$ is related to the intensity of the emission modulated at 2ω . These expressions show that the emission intensity for the resonant pump and probe waves ($\Delta_1 = \Delta_2 = 0$) increases first then decreases as the pump power increases.

III. RESULTS AND DISCUSSION

The theoretical expressions for the probe amplification profiles have complicated forms which are necessary to understand the atomic behavior with a widely changed parameter. We give numerical results of the Fourier amplitudes of ρ_{21} in Eqs. (18) and (20) and analytical forms for extreme cases to gain the implications of the line-shape characteristics. To avoid further complications we consider the case of the zero pump detuning $\omega_1 = \omega_{10}$ in the following calculation. We also assume that the decay rates of the levels are such that $\gamma_0 = \gamma_2 = 0.1$ and $\gamma_1 = 1.0$ and those for the off-diagonal elements are pure radiative, i.e., $\gamma_{ij} = (\gamma_i + \gamma_j)/2$ ($i=0,1,2$).

We first discuss β_0 , the Fourier amplitude at ω_2 . Inserting β_0 into Eq. (5), we get the gained power in the probe wave due to amplification in the four-wave-mixing process. In Fig. 2, we have displayed the pump power dependence of β_0 for the pump-frequency difference $\omega = 2\gamma_{10}$. At a low pump intensity ($V_{10} < 2\gamma_{10}$), the line profile is composed of two sharp resonances at the probe detuning $\Delta_2 = \pm\omega$. In that case the line shape is described by the equation obtained at the lowest-order perturbation calculation

$$\beta_0 = \beta_{+0} + \beta_{-0}, \quad (34)$$

where

$$\beta_{\pm 0} = iV_{10}^2 V_{20} \{ (2\gamma_{10}/\gamma_1) / [\gamma_{10} - i(\Delta_1 \pm \omega)] + 1 / [\gamma_{20} + i(\Delta_3 \pm \omega)] \} (\gamma_{21} + i\Delta_2)^{-1} \times [\gamma_{10} + i(\Delta_1 \pm \omega)]^{-1}.$$

The first term in the braces in Eq. (34) comes from step-

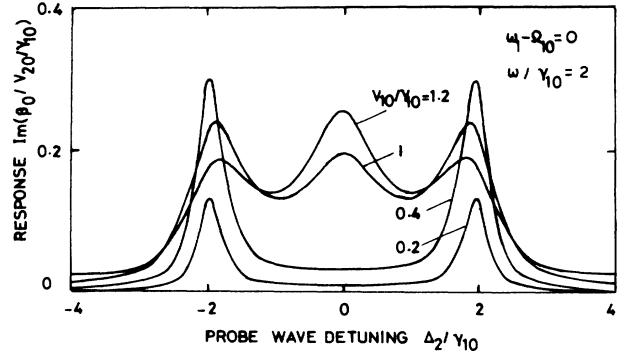


FIG. 2. The response at ω_2 is shown as a function of the probe detuning for the pump frequencies $\omega_1 \pm \omega = \Omega_{10} \pm 2\gamma_{10}$.

wise transition, while the second comes from the two-photon transition.

As the pump intensity increases, a broad resonance at the line center appears. The resonance is due to the mixing contributions of higher-frequency components induced in ρ_{21} .

For small pump-frequency separation $\omega \ll \gamma_{10}$, we depict $\beta_0(\Delta_2)$ in Fig. 3. The line profile is single peaked at a low pump intensity, whereas it has, in the saturation regime, three peaks located at the line center and the Rabi frequencies. The resonance at the line center comes from the interference of the two processes shown in Figs. 1(a) and 1(b).

The Fourier amplitudes β_2 and β_{-2} give rise to light generation due to four-wave mixing induced by the three waves at frequencies $\omega_1 \pm \omega$ and ω_2 . The generated wave is detected as a beat note with frequency 2ω against E_2 .

From Eq. (22), the beat intensity at the frequency 2ω is

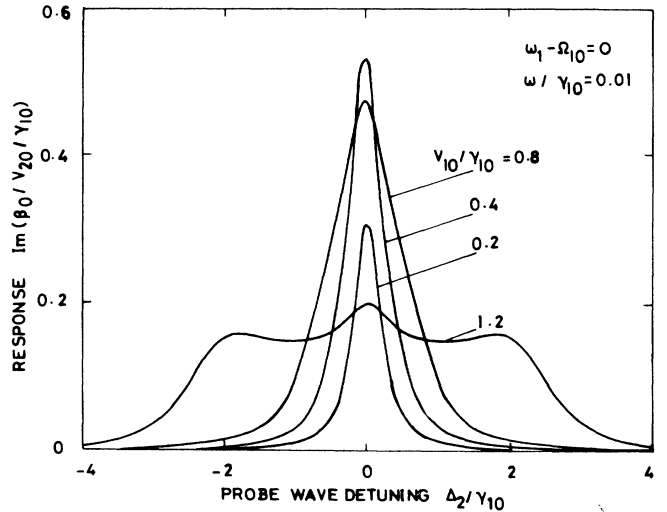


FIG. 3. The response at ω_2 is shown as a function of the probe detuning for the two-pump frequencies $\omega_1 \pm \omega = \Omega_{10} \pm 0.01\gamma_{10}$.

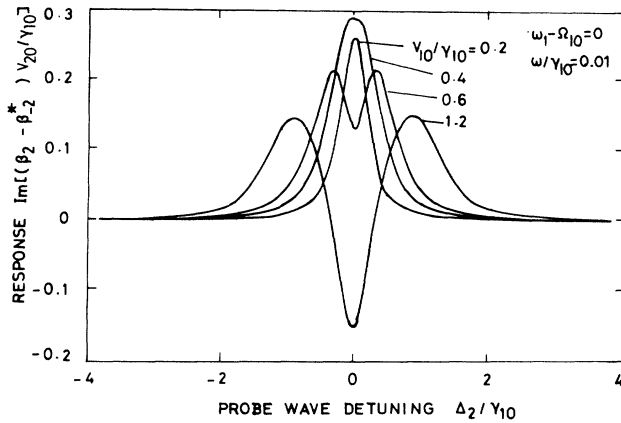


FIG. 4. The response modulated at 2ω is shown as a function of the probe-wave detuning for the pump frequencies $\omega_1 \pm \omega = \Omega_{10} \pm 0.01\gamma_{10}$, in the case where the phase difference between the pump field envelope and the signal is zero.

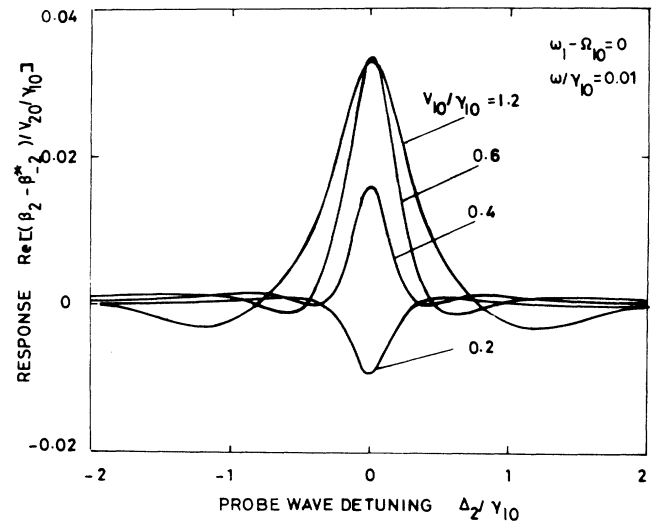


FIG. 5. The response modulated at 2ω is shown as a function of the probe detuning for the same pump frequencies as those in Fig. 4 in the case where the phase difference is $\pi/2$.

proportional to

$$\text{Im}[(\beta_2 - \beta_{-2}^*)e^{2i\omega t}] = |\beta_2 - \beta_{-2}^*| \cos(2\omega t + \psi_p), \quad (35)$$

where the power-dependent phase ψ_p is

$$\psi_p = \tan^{-1}[\text{Im}(\beta_2 - \beta_{-2}^*) / \text{Re}(\beta_2 - \beta_{-2}^*)]. \quad (36)$$

The signal consists of two components that vary as $\cos 2\omega t$ and $\sin 2\omega t$. To measure the beat note, we adopt a phase-sensitive detection in which amplitudes of the two components can be detected separately. As typical examples, we illustrate the numerical results for the imaginary and the real parts of $\beta_2 - \beta_{-2}^*$ in Figs. 4 and 5, respectively. The former is proportional to the amplitude of the cosine component, while the latter is to the amplitude of the sine component.

$$\beta_{\pm 2} = \pm i V_{10}^2 V_{20} \{ 2[(\gamma_{10} \pm i\omega) / (\gamma_1 \pm 2i\omega)] / [\gamma_{10} - i(\Delta_1 \mp \omega)] + 1 / [\gamma_{20} + i(\Delta_3 \pm \omega)] \} [\gamma_{10} + i(\Delta_1 \pm \omega)]^{-1} [\gamma_{21} + i(\Delta_2 \pm 2\omega)]^{-1}, \quad (37)$$

in which the first term in the square brackets comes from a coherent population oscillation.²¹ Inserting Eq. (37) into Eq. (35), we have at $\Delta_1 = 0$ analytical forms of the line shapes for the cosine and the sine components of the beat notes as

$$\text{Im}(\beta_2 - \beta_{-2}^*) = 2V_{10}^2 V_{20} [(\gamma_{20}\gamma_{21} - \Delta_2^2)(\gamma_{20}^2 + \Delta_2^2) + (\Delta_2^2 + \gamma_{20}\gamma_{21})\omega^2] / \{ \gamma_{10}(\gamma_{21}^2 + \Delta_2^2)[(\gamma_{20}^2 - \omega^2 + \Delta_2^2)^2 + 4\omega^2\gamma_{20}^2] \}, \quad (38a)$$

and

$$\text{Re}(\beta_2 - \beta_{-2}^*) = -2\omega V_{10}^2 V_{20} [(\gamma_{21} - 2\gamma_{20})\Delta_2^2 - \gamma_{21}(\gamma_{20}^2 + \omega^2)] / \{ 2\gamma_{10}(\gamma_{21}^2 + \Delta_2^2)[(\gamma_{20}^2 - \omega^2 + \Delta_2^2)^2 + 4\omega^2\gamma_{20}^2] \}. \quad (38b)$$

In the limiting case $\omega \ll \gamma_{20}$, the linewidth for the cosine component is γ_{20} , while that for the sine component is reduced to $0.41\gamma_{20}$, which is smaller than the two-photon resonance linewidth γ_{20} .

In the other limiting case of a small pump-frequency separation, $\omega \ll \gamma_{20}$, the analytical expressions for the

The line profile of the cosine component is a Lorentzian curve with a narrow width at a low pump intensity. As the intensity increases, the profile shows saturation with a broadened linewidth and then peak splitting. For $V_{10} = 0.3\gamma_{10}$, the sign of the value at $\Delta_2 = 0$ is reversed with respect to the value for a lower pump intensity.

For the sine component, the line profile has smaller peak value and narrower width compared with the cosine component. The linewidth becomes broader and the sign of the value at the line center is reversed as the pump intensity is increased. The linewidths can be estimated by the calculation in two limiting cases as discussed in the following.

We first examine the behavior of the beat at a low pump intensity. The calculation of Eqs. (20a) and (20b) for lowest order in V_1 gives

line shape can be obtained by solving ρ_{21} . For the latter case, the atomic response follows the slowly varying envelope of the pump field as if the amplitude were constant at every moment.²²

Then, we may use the density-matrix element^{23,24} ρ_{21} , which is given by (see Appendix A)

$$(\rho_{21})_{\text{slow}} = \frac{2i\gamma_0 V_1^2 V_{20} (\Gamma + i\Delta_2) \exp(-i\omega_2 t)}{\gamma_{10} (\gamma_0 \gamma_1 + 4V_1^2) [V_1^2 + (\gamma_{21} + i\Delta_2)(\gamma_{20} + i\Delta_2)]}, \quad (39)$$

with $V_1 = V_{10} \sin \omega t$. The envelope of $(\rho_{21})_{\text{slow}}$ can be decomposed into a Fourier series as

$$(\rho_{21})_{\text{slow}} = (C_0 + C_2 \cos 2\omega t + C_4 \cos 4\omega t + \dots) \times \exp(-i\omega_2 t), \quad (40)$$

where

$$C_n = (\omega/2\pi) \int_{-\pi/\omega}^{\pi/\omega} (\rho_{21})_{\text{slow}} \cos 2n\omega t dt. \quad (41)$$

In the limit $\omega \ll \gamma_{20}$ and $V_{10} \gg \gamma_{20}$, the imaginary part of the Fourier amplitude C_n are given by (see Appendix B)

$$\begin{aligned} \text{Im}C_0 \simeq -\text{Im}C_2 \simeq & (\gamma_0 \Gamma V_{20} / 2^{3/2} \gamma_{10} V_{10}) \\ & \times [(\Delta_2^2 + \gamma_{20}^2)(\Delta_2^2 + \gamma_{21}^2)]^{1/4} \\ & \text{for } |\Delta_2| < \gamma_{20} \end{aligned} \quad (42a)$$

and

$$\begin{aligned} \text{Im}C_0 \simeq \text{Im}C_2 \simeq & (\gamma_0 \Gamma V_{10} V_{20} / 2\gamma_{10}) \\ & \times [(V_{10}^2 - \Delta_2^2)^2 + V_{10}^2 (\gamma_{20} + \gamma_{21})^2]^{-3/4} \\ & \text{for } |\Delta_2| \sim V_{10}. \end{aligned} \quad (42b)$$

These expressions show the heights and the positions of the resonances for the amplified probe wave and the generated wave at $\omega_2 \pm 2\omega$. The Fourier amplitudes C_0 and C_2 have resonances at $\Delta_2 = 0, \pm V_{10}$. The resonances are due to the time variations of the pump field amplitude in the beat note. The resonance at $\Delta_2 = 0$ comes from the generation at the time region $t \approx n\pi/\omega$ ($m = 0, 1, 2, \dots$) when the pump-wave amplitude is at a low-intensity level, while the resonances at $\Delta_2 = \pm V_{10}$ are due to wave generation at time $t \approx (2n+1)\pi/2\omega$, when the field intensity of the pump wave is high.

In Figs. 4 and 5, the sign of C_2 at $\Delta_2 = 0$ becomes reversed as the pump intensity increases. The imaginary and the real parts of $\beta_2 - \beta_{-2}^*$ are estimated by the Fourier amplitudes in Eqs. (38) for the limiting case $\omega \ll \gamma_{20}$. The origin of the peak-value change at $\Delta_2 = 0$ is the ac Stark shift in the energy levels 0 and 1. Because of the shift, the probe field with ω_2 is deviated from the resonance condition $\omega_2 - \Omega_{21} = 0$. The deviation increases as

$$\langle \beta_{\pm 2} \rangle = \frac{2\sqrt{\pi} V_{10}^2 v_{20}}{\epsilon k_2 u} \frac{1}{\Delta_1 \pm (2\epsilon r_k + 1)\omega + \epsilon r_k [\Delta_2 - i\Gamma_0(\epsilon)]} \left[\frac{1}{\gamma_1 \pm 2i\omega} - \frac{i}{\Delta_1 \pm (2\epsilon r_k - 1)\omega + (\epsilon r_k - 2)[\Delta_2 - i\Gamma_1(\epsilon)]} \right], \quad (47)$$

where

$$\Gamma_0(\epsilon) = \epsilon r_k \gamma_{10} + \gamma_{21}$$

and

$$\Gamma_1(\epsilon) = [(1 - \epsilon r_k) \gamma_{21} + \epsilon r_k \gamma_{20}] / (1 - 2\epsilon r_k),$$

the pump intensity increases. For the sinusoidal variation of the pump intensity, the signal intensity changes as follows. When the pump intensity has a maximum value, $\beta_2 - \beta_{-2}^*$ at $\Delta_2 = 0$ is lowered in its magnitude due to a large deviation from the resonant condition, while $\beta_2 - \beta_{-2}^*$ at $\Delta_2 = 0$ is large for a lower pump intensity. Thus the beat intensity at 2ω varies as if it had a phase shifted by $\pi/2$ from the sinusoidal time variation of the pump intensity.

We next consider four-wave mixing in a gaseous medium composed of a Doppler-broadened atomic system, in the case where the propagation directions of the waves influence the emission intensity. Then we assume that the pump and the probe waves either copropagate or counterpropagate in the z axis.

For an atom moving with V_z , the z component of the velocity, the frequency of the pump wave in the atomic rest frame, becomes

$$\omega_s = \omega_1 - k_1 v_z, \quad (43)$$

where $k_1 = \omega_1/c$.

The probe frequency becomes, in the copropagation configuration,

$$\omega_p = \omega_2 - k_2 v_z, \quad (44a)$$

and, in the counterpropagation configuration,

$$\omega_p' = \omega_2 + k_2 v_z, \quad (44b)$$

where $k_2 = \omega_2/c$.

We have a density matrix for the moving atom, replacing ω_1 and ω_2 in Eqs. (6) and (7) by ω_s and ω_p (ω_p'), respectively. To find the intensity of the generated wave in the atomic ensemble, we integrate over the velocity distribution for β_0 and β_2 in Eqs. (34) and (37) as

$$\langle \rho_{21} \rangle = \frac{1}{\sqrt{\pi} u} \int_{-\infty}^{\infty} dv_z \exp(-v_z^2/u^2) \rho_{21}(v_z), \quad (45)$$

when we assume the Maxwellian distribution with the mean thermal velocity u .

In the Doppler limit ($\gamma_i, \gamma_{ij} \ll k, u, k_2 u$), we perform the integral in Eq. (45) using the residue technique, having

$$\langle \beta_{\pm 0} \rangle = \frac{2\sqrt{\pi} V_{10}^2 v_{20}}{\epsilon k_2 u} \frac{1}{\Delta_1 + \omega + \epsilon r_k [\Delta_2 - i\Gamma_0(\epsilon)]} \times \left[\frac{1}{\gamma_1} - \frac{1}{\Delta_1 + \omega + (\epsilon r_k - 2)[\Delta_2 - i\Gamma_1(\epsilon)]} \right] \quad (46)$$

and

with $r_k = k_2/k_1$ and $\epsilon = \pm 1$. Here $\epsilon = 1$ for copropagating waves and $\epsilon = -1$ for counterpropagating waves.

From Eqs. (46) and (47) we have curves of emission intensity versus the probe detuning Δ_2 . The linewidths of the curves depend on dephasing rates, wave propagation

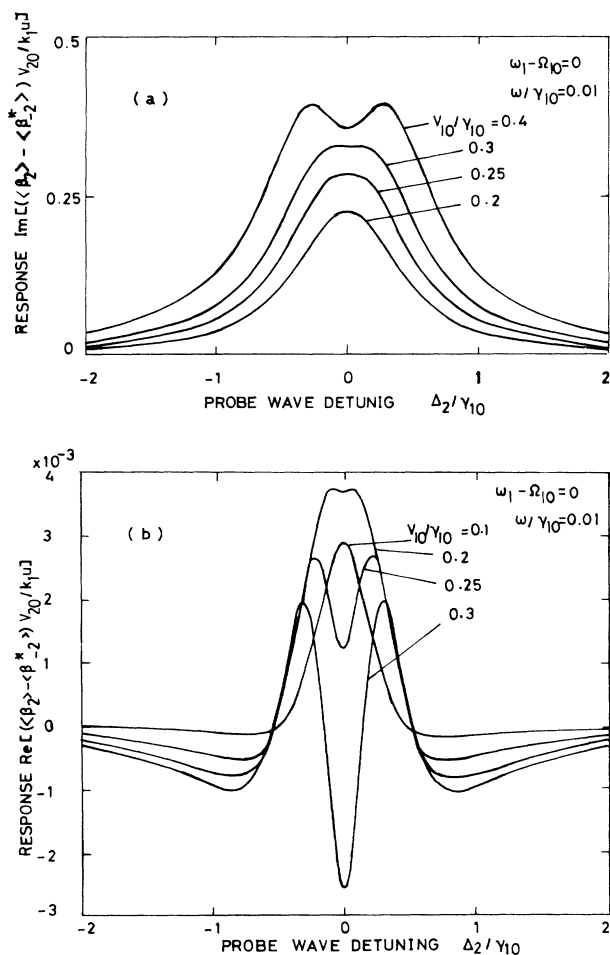


FIG. 6. Intensity of the generated wave for a Doppler-broadened atomic system as a function of the probe detuning Δ_2 . The line shapes are calculated in the Doppler limit for several pump intensities, using the following parameters: $k_2/k_1=0.8$, $\Delta_1=0$, and $\omega/\gamma_{10}=0.01$. (a) The cosine component, $\text{Im}(\langle\beta_2\rangle - \langle\beta_2^*\rangle)$, for $I_1/\gamma_{10}=0.2, 0.25, 0.3$, and 0.4 ; (b) the sine component, $\text{Re}(\langle\beta_2\rangle - \langle\beta_2^*\rangle)$ for $I_1/\gamma_{10}=0.1, 0.2, 0.25$, and 0.3 .

directions, and wave-number ratio of the pump and the probe waves.

One of the interesting cases is copropagation configuration, where the Doppler cancellation occurs for $k_1 \approx k_2$ and $\epsilon=1$. The effect of the cancellation can be predominantly observed in the sine component of the emission intensity modulated at 2ω . At a low pump intensity the linewidth of the sine component is approximately equal to γ_{20} .

For an arbitrary pump intensity, we calculate numerically for copropagating waves with $\Delta_1=0$, $\omega=0.01\gamma_{10}$, and $k_2/k_1=0.8$. The results are plotted in Fig. 6. Compared with the cosine component, the sine component has a narrower linewidth. As the pump intensity increases, line shapes become double peaked, and then in the line shape of the sine component, a sharp resonance

with a negative value appears at $\Delta_2=0$, as in the case of atoms at rest.

IV. CONCLUSION

The saturation characteristics of four-wave mixing were investigated in a three-level system coupled to a two-frequency pump wave and a weak probe wave. Especially the line shape of the emitted field was examined at high pump intensities, where the line shape reveals power broadening, phase shifts, and peak splitting.

A wave emitted in the direction of the probe beam makes a beat against the probe wave. The beat signal can be obtained by a lockin amplifier with reference signal at the modulation frequency of the pump field amplitude. The line shape obtained for the probe detunings is, therefore, modified by the phase difference between the detection system and the modulation frequency. The linewidth which is narrower than that for the two-photon absorption is obtained when the phase of the detection system is adjusted to be $\pi/2$ shifted from the reference signal of the pump-wave envelope. The subnatural linewidth predicted by our calculation will be useful for the frequency stabilization as well as high-resolution spectroscopy.

The response in a Doppler-broadened system was obtained by integrating over its velocity distribution. In the copropagation configuration of the pump and the probe waves, the emission line shape has a narrow width due to partial Doppler compensation. As the pump power increases, the line shape changes into a two-peaked spectrum similar to that for atoms at rest.

Hackel and Ezekiel²⁵ reported, in a two-step scattering of iodine, a split structure due to the ac Stark effect at much higher saturating pump power. The central dip of the observed line shape will have the same origin as the one we discussed.

The generated wave also shows multiphoton scattering characteristics. As the pump intensity increases, the waves at frequencies $\omega_2 \pm 4\omega, \omega_2 \pm 6\omega, \dots$, are generated simultaneously due to higher-order processes. The properties of the waves could be obtained by the analysis of higher-frequency Fourier components of ρ_{21} in such a way as that discussed above.

ACKNOWLEDGMENTS

The author wishes to thank T. Kasuya for his interest and useful discussions.

APPENDIX A

We solve the density-matrix elements in Eqs. (4a)–(4i) for a strong pump wave with constant amplitude, when the probe wave is assumed to be of small perturbation. Under the assumption, we calculate the density-matrix elements, neglecting the probe wave E_2 , as

$$\rho_{00} = \gamma_1(\gamma_0|\gamma_{10} + i\Delta_1|^2 + 2\gamma_{10}V_1^2)/D, \quad (\text{A1})$$

$$\rho_{11} = 2\gamma_0\gamma_1V_1^2/D, \quad (\text{A2})$$

$$\rho_{10} = -i\gamma_0\gamma_1V_1(\gamma_{10} - i\Delta_1)/D, \quad (\text{A3})$$

with $D = \gamma_0 \gamma_1 |\gamma_{10} + i\Delta_1|^2 + 4\gamma_{10}^2 V_1^2$.

Inserting Eqs. (A1)–(A3) into Eqs. (4e) and (4f), we have the density-matrix element ρ_{21} , to the first order in E_2 ,

$$\rho_{21} = \frac{2i\gamma_0 V_1^2 V_2 (\Gamma + i\Delta_2) \exp(-i\omega_2 t)}{\gamma_{10} (\gamma_0 \gamma_1 + 4V_1^2) [V_1^2 + (\gamma_{21} + i\Delta_2)(\gamma_{20} + i\Delta_2)]} . \quad (\text{A4})$$

APPENDIX B

We deduce approximate analytical forms for the Fourier components of the induced polarization at the probe frequency for the case where the pump wave has a slowly varying amplitude.

We consider the limiting case, $V_1^2 \gg \gamma_{20}\gamma_{21}$, for $n=0$ and 2 in the following. If we replace the imaginary part of the Fourier amplitudes in Eq. (40) by

$$\text{Im}C_n = (\gamma_0 \Gamma V_{20} / 8\gamma_{10} V_{10}^2) f_n , \quad (\text{B1})$$

and perform the integration in Eq. (41), we have

$$f_n(\Delta_2) \simeq \int_{-1}^1 \frac{x^{n/2}}{(x-\epsilon)^2 + \delta^2} \frac{1-x}{1+x} dx, \quad n=0,2 \quad (\text{B2})$$

with $\epsilon = 1 - (\Delta_2^2 - \gamma_{20}\gamma_{21}) / V_{10}^2$ and

$$\delta = [(\gamma_{20} + \gamma_{21})\Delta_2] / V_{10}^2 .$$

The evaluation of the integral in Eq. (B2) can be performed analytically in four regions of detuning, $\Delta_2^2 \ll \gamma_{20}\gamma_{21}$, $\gamma_{20}\gamma_{21} \ll \Delta_2^2 \ll 4V_{10}^2$, $\Delta_2^2 \approx V_{10}^2$, and $\Delta_2^2 \gg V_{10}^2$.

First, for $\Delta_2^2 \ll \gamma_{20}\gamma_{21}$, we have $\epsilon \simeq 1$ and $|\delta| \ll 1$. The region of the dominant contribution to the integral in Eq. (B2) is $|x - \epsilon| \simeq |\delta|$. The integral is evaluated as

$$f_0 \simeq \frac{1}{\sqrt{2}} \int_{-1}^1 \frac{(1-x)^{1/2}}{(x-1)^2 + (\epsilon-1)^2 + \delta^2} dx \simeq \frac{1}{2} [(\epsilon-1)^2 + \delta^2]^{-1/4} \quad (\text{B3})$$

and

$$f_2 \simeq f_0 . \quad (\text{B4})$$

Second, for $\Delta_2^2 \gg \gamma_{20}\gamma_{21}$ and $\Delta_2^2 \ll V_{10}^2$, the region $|x - \epsilon| \lesssim \delta$ contributes dominantly to the integral. Equations (B2) are

$$f_0(\Delta_2) \simeq \frac{1-\epsilon}{1+\epsilon} \int_{-1}^1 \frac{dx}{(x-\epsilon)^2 + \delta^2} dx \simeq (1/|\delta|)(1-\epsilon)/(1+\epsilon) \quad (\text{B5})$$

and

$$f_2(\Delta_2) \simeq f_0(\Delta_2) . \quad (\text{B6})$$

Third, for $\Delta_2^2 \approx V_{10}^2$, especially $V_{10}(\gamma_{20} + \gamma_{21}) \gg |V_{10}^2 - \Delta_2^2|$, where the contribution from the region $-1 + |\epsilon| > x > -1$ is dominant, we get

$$f_0(\Delta_2) \simeq (2^{1/2}/\pi) \int_{-1}^1 \frac{1}{(x+1)^2 + (\epsilon+1)^2 + \delta^2} \frac{dx}{(1+x)^{1/2}} \simeq \frac{1}{2} [(\epsilon+1)^2 + \delta^2]^{-3/4} \quad (\text{B7})$$

and

$$f_2(\Delta_2) \simeq f_0(\Delta_2) . \quad (\text{B8})$$

Fourth, for $\Delta_2^2 \gg V_{10}^2$, Eq. (B2) is approximately as

$$f_0(\Delta_2) \simeq \int_{-1}^1 \frac{1}{[x + (\epsilon^2 + \delta^2)]} \frac{1-x}{1+x} dx \simeq 1/(\epsilon^2 + \delta^2) , \quad (\text{B9})$$

and

$$f_2(\Delta_2) \simeq 1/[2(\epsilon^2 + \delta^2)] . \quad (\text{B10})$$

From Eqs. (B3)–(B10), we see that Eq. (B2) has extrema at $\Delta_2=0$ and $\pm V_{10}$, noting that Eq. (B2) is a smooth function of Δ_2 .

Inserting Eqs. (B3), (B4), (B7), and (B8) into Eq. (B1), we obtain Eqs. (42).

¹R. L. Carman, R. Y. Chiao, and P. L. Kelley, Phys. Rev. Lett. **17**, 1281 (1966).

²P. P. Sorokin, M. M. T. Loy, and J. R. Lankard, IEEE J. Quantum Electron. **QE-13**, 871 (1977); A. V. Smith and J. F. Ward, *ibid.* **QE-17**, 525 (1981); R. W. Boyd, M. G. Raymer, P. Narum, and D. J. Harter, Phys. Rev. A **24**, 411 (1981).

³D. G. Steel and J. F. Lam, Phys. Rev. Lett. **43**, 1588 (1979).

⁴P. Aubourg, J. P. Bettini, G. P. Agrawal, P. Cottin, D. Guerin, O. Meunier, and J. L. Boulnois, Opt. Lett. **6**, 383 (1981).

⁵R. G. DeVoe and R. G. Brewer, Phys. Rev. A **26**, 705 (1982).

⁶Y. Prior and E. Yarkoni, Phys. Rev. A **28**, 3689 (1983).

⁷N. Tanno, K. Ohkawara, and H. Inaba, Phys. Rev. Lett. **46**, 1282 (1981); R. W. Boyd, M. S. Malcuit, D. J. Gauthier, and K. Rzazewski, Phys. Rev. A **35**, 1648 (1987).

⁸G. Camy, Ch. J. Borde, and M. Ducloy, Opt. Commun. **41**, 325

(1982).

⁹M. Ducloy and D. Bloch, J. Phys. **43**, 57 (1982).

¹⁰R. K. Raj, D. Bloch, J. J. Synder, G. Camy, and M. Ducloy, Phys. Rev. Lett. **44**, 1251 (1980).

¹¹P. Ye and Y. R. Shen, Phys. Rev. A **25**, 2183 (1982).

¹²G. S. Agarwal, Phys. Rev. A **34**, 4055 (1986).

¹³G. S. Agarwal and R. W. Boyd, Phys. Rev. A **38**, 4019 (1988).

¹⁴M. D. Reid and D. F. Walls, Phys. Rev. A **34**, 4929 (1986).

¹⁵M. Ducloy, F. A. M. de Oliveira, and D. Bloch, Phys. Rev. A **32**, 1614 (1985).

¹⁶P. Verkerk, M. Pinard, and G. Grynberg, Phys. Rev. A **34**, 4008 (1986).

¹⁷M. Pinard, P. Verkerk, and G. Grynberg, Phys. Rev. A **35**, 4679 (1987).

¹⁸S. Stenholm and W. E. Lamb, Jr., Phys. Rev. **181**, 618 (1969).

- ¹⁹B. J. Feldman and M. S. Feld, *Phys. Rev. A* **1**, 1375 (1970);
Phys. Rev. A **5**, 899 (1972).
- ²⁰S. Y. Yee, T. K. Gustafson, S. A. J. Druet, and J.-P. E. Taran,
Opt. Commun. **23**, 1 (1977).
- ²¹J. J. Song, J. H. Lee, and M. D. Levenson, *Phys. Rev. A* **17**,
1439 (1978).
- ²²B. Couillaud, A. Ducasse, and A. Dienes, *Appl. Phys.* **16**, 359
(1978).
- ²³S. Feneuille and M.-G. Schweighofer, *J. Phys. (Paris)* **36**, 53
(1975).
- ²⁴M. Tsukakoshi and K. Shimoda, *Jpn. J. Appl. Phys.* **19**, 615
(1980).
- ²⁵R. P. Hackel and S. Ezekiel, *Phys. Rev. Lett.* **42**, 1736 (1979).